Project report for final year project in Physics & Astronomy

Visualising the Abraham-Minkowski Light Field Momentum

Matriculation Number: 200007312

Mateo Guzmán Subiría

Module: PH5101 MPhys Physics

Science is often highly collaborative. Please clarify here which parts of the work reported have been done by you and which parts include the work of others. For example, this might include provision of simulation or analysis codes which you utilised or modified, provision of experimental data to analyse, collaborations with others in performing new measurements, if you built up things from scratch in your project or started from pre-existing setups, and others. Providing this information helps clarify the scope and focus of your project work.

The code and results have been produced from scratch under the supervision of Dr Michael Mazilu.

Acknowledgements

I want to express my gratitude to my supervisor, Dr Michael Mazilu, for all the time and guidance he has provided me during the whole project. I also wish to thank my friends and family for their unwavering support not only during my dissertation but throughout my time in St Andrews.

Abstract

The current work deals with the development of computational tools to visualise the field momentum of light waves travelling in dielectric media with a focus on identifying phenomena related to Abraham and Minkowski's formulations of the electromagnetic momentum which are at the core of the eponymous controversy. Our approach consists in simulating optical media as 1D photonic crystals composed of periods of thin medium and vacuum layers with the latter being proportionately much smaller. We represent the layers as matrices and, by employing the transfer matrix method, we produce the forwards and backwards propagating mode field amplitudes and phases for a light pulse composed of singly polarised plane waves at normal incidence. We simulate two optical systems: one corresponds to 2 crystals sandwiched between a vacuum section and a distributed Bragg reflector structure acting as a mirror, and the other corresponds to the same crystals between two vacuum sections. In both cases, we compute the Maxwell stress tensor at the vacuum layers and the Lorentz force acting on the bulk of the medium layers. This allows the calculation of the momentum flux and the accumulated impulse surface density in the systems through two different methods. Our findings show transient disagreements between the calculations, with the Lorentz method producing smaller impulse surface densities and showing greatest variation at the boundaries between crystals. However, in the long-time limit, after the pulse has exited the systems, both methods converge exactly to the same impulse surface densities for the dehomogenised media, but differ for the DBR. The transient disagreement can be explained by the non-uniqueness of the Maxwell stress tensor.

Keywords: Electromagnetic momentum, optical momentum, Maxwell stress tensor, Lorentz force, photonic crystals, stratified media, transfer matrix method, scattering matrices, computational simulations

Contents

Glossary

boundary

The limit between *crystals* or *periods* which lies at the middle of the vacuum *layers* (**NOT** to be confused with *interface*).

crystal

The *photonic crystal* used to simulate a dehomogenised dielectric medium (**NOT** to be confused with *medium*).

element

Each of the components (*layer* or *interface*) that compose a *period*.

interface

The limit between *layers* inside a *period* (**NOT** to be confused with *boundary*).

layer

Either *medium* or vacuum which makes up a part of a *period* in a *photonic crystal*.

medium

Refers to the medium portion/layer in a *period* **NOT** a *crystal*.

period

The basis structure of the *photonic crystal*s composed of a vacuum *layer*, an *interface*, a *medium layer*, an *interface*, and a vacuum *layer* as illustrated in fig. 3.1.

photonic crystal

A highly ordered material that possesses a periodically modulated dielectric constant.

List of Acronyms

DBR	distributed Bragg reflector
EM	electromagnetic
EMSET	electromagnetic stress-energy tensor
MEs	Maxwell's equations
MST	Maxwell stress tensor
PC	photonic crystal
PW	plane wave
TMM	transfer matrix method

List of Symbols

Symbol	Description	Units
μ_0	vacuum permeability	$\mathrm{kg\,m\,s^{-2}\,A^{-2}}$
ε_0	vacuum permittivity	$\mathrm{A^2\,s^4\,kg^{-1}\,m^{-3}}$
$\mathbf{E}$	electric field	$\mathrm{kg\,m\,s^{-3}\,A^{-1}}$
$\mathbf{D}$	displacement field	$\mathrm{A\,s\,m^{-2}}$
$\mathbf{P}$	polarisation density	$\mathrm{A\,s\,m^{-2}}$
$\mathbf{B}$	magnetic field	$\mathrm{kg\,s^{-2}\,A^{-1}}$
$\mathbf{H}$	auxiliary magnetic field	$\mathrm{A\,m^{-1}}$
$\mathbf{J_b}$	bound volume current density	$\mathrm{A\,m^{-2}}$
$\overleftrightarrow{\mathbf{T}}$	Maxwell stress tensor	$\mathrm{kg\,m^{-1}\,s^{-2}}$
$\mathbf{f_s}$	force surface density	$\mathrm{kg\,m^{-1}\,s^{-2}}$
$\mathbf{S}$	Poynting vector	$\mathrm{kg\,s^{-3}}$
$\mathbf{g}$	EM momentum density	$\mathrm{kg\,m^{-2}\,s^{-1}}$
$\mathbf{\Pi}$	momentum flux	$\mathrm{kg\,m^{-1}\,s^{-2}}$
$\Delta\eta^z$	impulse surface density along $\hat{\mathbf{z}}$	$\mathrm{kg\,m^{-1}\,s^{-1}}$
$\mathbf{k}$	wavevector	$\mathrm{m^{-1}}$
k	wavenumber	$\mathrm{m^{-1}}$
ω	angular frequency	$\mathrm{rad\,s^{-1}}$
$\mathbf{E_0}$	E-field amplitude	$\mathrm{kg\,m\,s^{-3}\,A^{-1}}$
$\mathbf{B_0}$	B-field amplitude	$\mathrm{kg\,s^{-2}\,A^{-1}}$
c	speed of light (in vacuum)	$\mathrm{m\,s^{-1}}$
a	forward propagating mode	$\mathrm{kg\,m\,s^{-3}\,A^{-1}}$
b	backward propagating mode	$\mathrm{kg\,m\,s^{-3}\,A^{-1}}$
θ	angle of incidence	
h	period width	m
n	refractive index	
n_0	vacuum refractive index	
n_{eff}	effective refractive index	
n_m	medium layer refractive index	
n_{DBR}	DBR medium layer refractive index	
N_{per}	number of periods	
r	width ratio	

Bold unitalicised text denotes that an object is a vector. The double arrow overhead denotes that an object is a second order tensor. The double underlining denotes that an object is a matrix.

For our simulation, we work with arbitrary units, as we have set a number of physical constants (namely ε_0, μ_0, c) have been set to unity. Nonetheless, we show the units above and keep them in consideration for dimensional analysis.

1. Introduction

Comets' dust tails are formed under the action of solar radiation pressure [1]. This beautiful phenomenon illustrates that light – electric and magnetic fields – carries momentum which can be transferred to matter. Work on the theory of optical momentum and energy transfer to matter dates back to the end of the 19th century [2]. In recent years, it has regained interest, much of which can be attributed to the growth in nanotechnology where it finds practical applications [3].

In vacuum, the electromagnetic (EM) momentum density $\mathbf{g}$ is unambiguously

$$\mathbf{g} = \varepsilon_0 \mathbf{E} \times \mathbf{B} \tag{1.1}$$

as proposed by Poynting [4], where $\mathbf{E}$ is the electric field, $\mathbf{B}$ is the magnetic field and ε_0 is the free space permittivity. However, what happens when light travels in a dielectric medium? Matter is subject to polarisation and magnetisation, which modify the effective electric and magnetic fields. Hence, the effective field momentum is modified.

In the early 1900s, Abraham [5] and Minkowski [6] developed two opposing expressions based on classical electrodynamics and relativistic theory, which are at the core of the controversy that shares their names. Abraham worked with a symmetric, but not relativistically invariant, electromagnetic stress-energy tensor (EMSET) resulting in an EM momentum density n times larger in a medium with refractive index n. Meanwhile, Minkowski worked with a relativistically invariant, but not symmetric, EMSET resulting in a momentum density n times smaller [3, 7]. This difference by a factor of n^2 disappears in free space where their EMSETs converge to the same uncontested expression. During the 20th and 21st centuries, there have been multiple theoretical [3, 7, 8, 9, 10, 11] and experimental [7, 9, 12, 13, 14, 15] attempts to resolve the controversy.

The goal of this project is not to develop a resolution, but rather to produce computational tools that enable us to visualise EM fields and their momenta as they propagate through dielectric media. In particular, we aim to identify any behaviour predicted by the main theories described above. The optical systems that we simulate, namely a pulse travelling through different *photonic crystal* (PC) systems with a) a mirror and b) vacuum at the end, draw inspiration from the thought experiments relayed by Griffiths in his 2012 review [16].

2. Theoretical Background

2.1 Maxwell's Equations (microscopic)

Maxwell's equations (MEs) describe the behaviour of electric and magnetic fields in space and time. In the microscopic regime, they describe EM fields at a fundamental level considering individual charges and currents between which there is free space. These are defined as [17]

$$\nabla \cdot \mathbf{E} = \frac{\rho}{\varepsilon_0} \tag{2.1}$$

$$\nabla \cdot \mathbf{B} = 0 \tag{2.2}$$

$$\nabla \times \mathbf{E} = -\frac{\partial \mathbf{B}}{\partial t} \tag{2.3}$$

$$\nabla \times \mathbf{B} = \mu_0 \mathbf{J} + \mu_0 \varepsilon_0 \frac{\partial \mathbf{E}}{\partial t} \tag{2.4}$$

where ρ is the volume charge density, $\mathbf{J}$ is the volume current density, and ε_0 and μ_0 are respectively the vacuum permittivity and permeability.

2.2 What Happens in Dielectrics? (macroscopic MEs)

At larger scales, where materials can be treated as continuous media, the effects of individual charges or currents are averaged and replaced with polarisation and magnetisation densities which modify the effective EM fields. The media are characterised by permittivities ε and permeabilities μ different than those in free space. Here, the "macroscopic" MEs come into play and the form they take depends on the particular properties of the media. As did Abraham and Minkowski [9], we deal with linear dielectrics, further assuming that the dielectrics we simulate are non-magnetisable, so $\mu = \mu_0$. Thus, the relevant constitutive relations are [17]

$$\mathbf{D} = \varepsilon \mathbf{E} \tag{2.5}$$

$$\mathbf{P} = \mathbf{D} - \varepsilon_0 \mathbf{E} = (\varepsilon - \varepsilon_0)\mathbf{E} \tag{2.6}$$

$$\mathbf{H} = \frac{\mathbf{B}}{\mu_0} \tag{2.7}$$

where $\mathbf{P}$ is the polarisation density, $\mathbf{D}$ is the displacement field, and $\mathbf{H}$ is the auxiliary magnetic field.

2.3 The Lorentz Force Law

The MEs, alongside the Lorentz force law $\mathbf{F} = \int_V (\rho\mathbf{E} + \mathbf{J} \times \mathbf{B})dV$ [18], where $\mathbf{F}$ is force, ρ is the charge density, $\mathbf{J}$ is the current density, and V is the integration volume; form the foundation of classical electromagnetic theory.

In the context of calculating the total force of radiation on a solid object, we present two formulations of the Lorentz force law as put forth by [19, 20, 21]

$$\mathbf{f_{v}}_1 = -(\nabla \cdot \mathbf{P})\mathbf{E} + \frac{\partial \mathbf{P}}{\partial t} \times \mathbf{B} \tag{2.8}$$

$$\mathbf{f_{v}}_2 = (\mathbf{P} \cdot \nabla)\mathbf{E} + \frac{\partial \mathbf{P}}{\partial t} \times \mathbf{B} \tag{2.9}$$

where $\mathbf{f_v}$ is a force volume density. We identify the term with the partial derivative as an induced bound volume current density $\mathbf{J_b}$.

2.4 The Maxwell Stress Tensor

The Maxwell stress tensor (MST) $\overleftrightarrow{\mathbf{T}}$ [22] is a second-order tensor that describes the distribution of EM forces per unit area acting on a surface. In free space,

$$\overleftrightarrow{\mathbf{T}} = \varepsilon_0 E_i E_j + \frac{1}{\mu_0} B_i B_j - \frac{1}{2}\left(\varepsilon_0 \mathbf{E} \cdot \mathbf{E} + \frac{1}{\mu_0}\mathbf{B} \cdot \mathbf{B}\right)\delta_{ij}. \tag{2.10}$$

where δ_{ij} is the Kronecker delta and $i, j = 1, 2, 3$ which in a Cartesian system correspond to directional components x, y, z. The MST corresponds to the lower right elements of the EMSET, which compactly expresses the conservation laws of linear momentum and energy in electromagnetism in 4D spacetime.

$\overleftrightarrow{\mathbf{T}}$ is related to the conservation of linear and angular momentum via the momentum continuity equation [23]

$$\nabla \cdot \overleftrightarrow{\mathbf{T}} = \mathbf{f_v} + \frac{1}{c^2}\frac{\partial \mathbf{S}}{\partial t}. \tag{2.11}$$

where $\mathbf{f_v}$ is the force (rate of mechanical momentum transfer) volume density, c is the speed of light in vacuum, and $\mathbf{S} = \mathbf{E} \times \mathbf{H} = \frac{1}{\mu_0}\mathbf{E} \times \mathbf{B}$ is the Poynting vector (EM energy flux). The last term gives the density of the rate of EM momentum being radiated away. By performing a volume integral on eqn. (2.11) and applying the Divergence Theorem, it is clear that integrating the MST over a closed surface delivers the force on that surface and the EM momentum flowing through it in the form of radiation. The MST is not uniquely defined. This is because the EMSET is only defined up to a divergence-free field i.e. we can add an arbitrary $\overleftrightarrow{\mathbf{T}}'$ such that $\nabla \cdot \overleftrightarrow{\mathbf{T}}' = -\frac{\partial \overleftrightarrow{\mathbf{T}}'}{\partial t}$ with no effect for the impulse from eqn. (2.11) in the long-time limit.

In the context of linear dielectrics, Abraham and Minkowski developed the same MST $\overleftrightarrow{\mathbf{T}} = E_i D_j + H_i B_j - \frac{1}{2}(\mathbf{E} \cdot \mathbf{D} + \mathbf{H} \cdot \mathbf{B})\delta_{ij}$ but formulated differing EM momentum densities $\mathbf{g}$. Minkowski's $\mathbf{g_M} = \mathbf{D} \times \mathbf{B}$ is developed on the identification of $\mathbf{g_M}$ as the difference between the total momentum density and the mechanical momentum density. Meanwhile, Abraham's

$\mathbf{g_A} = \frac{1}{c^2}\mathbf{E} \times \mathbf{H}$ arises from the assumption that $\mathbf{S}$ gives the field energy flux in the medium as well as in vacuum and the relation $\mathbf{S} = \mathbf{g}c^2$ from special relativity theory [7, 9] (note the relation with last term in eqn. (2.11)). However, several other different formulations of the MST have been put forth over the years [7]. Nevertheless, these expressions converge at eqn. (2.10) in vacuum.

2.4.1 Time Averaging

In this study, the fields we work with are complex, so we employ time-averaged expressions, whereby $E_i E_j = \frac{1}{2}(E_i{}^* E_j + E_i E_j{}^*)$. Therefore, $\overleftrightarrow{\mathbf{T}}$ in vacuum becomes

$$\overleftrightarrow{\mathbf{T}} = \frac{1}{2}\left[\varepsilon_0 \left(E_i{}^* E_j + E_i E_j{}^* - |\mathbf{E}|^2 \delta_{ij}\right) + \frac{1}{\mu_0}\left(B_i{}^* B_j + B_i B_j{}^* - |\mathbf{B}|^2 \delta_{ij}\right)\right]. \tag{2.12}$$

2.5 Plane Waves

Plane waves (PWs) are solutions to Maxwell's equations describing the propagation of EM fields through time and space. The EM fields take the form

$$\mathbf{E} = \mathbf{E_0^+} e^{i(\mathbf{k}\cdot\mathbf{Q}-\omega t)} + \mathbf{E_0^-} e^{-i(\mathbf{k}\cdot\mathbf{Q}-\omega t)} \tag{2.13}$$

$$\mathbf{B} = \mathbf{B_0^+} e^{i(\mathbf{k}\cdot\mathbf{Q}-\omega t)} + \mathbf{B_0^-} e^{-i(\mathbf{k}\cdot\mathbf{Q}-\omega t)} \tag{2.14}$$

where $\mathbf{k}$ is the wavevector, ω is the angular frequency, $\mathbf{E_0}$ and $\mathbf{B_0}$ are the amplitude vectors (pointing perpendicular to $\mathbf{k}$ and each other), $\mathbf{Q}$ is the position vector, and t is time [17]. The wavenumber $k = |\mathbf{k}|$ changes as a PW enters a medium with a different n, but ω remains unchanged as it is set by the (theoretical) source, not the medium. The dispersion relation

$$\mathbf{v}_\phi = \frac{\omega}{k}\hat{\mathbf{k}} \tag{2.15}$$

gives the phase velocity ($v_\phi = c$ in vacuum). In a dielectric medium, the phase velocity of this wave $\mathbf{v}_\phi = \frac{\hat{\mathbf{k}}}{\sqrt{\mu\varepsilon}}$, which coupled with the definition of the refractive index n [24]

$$n = \frac{c}{v_\phi} = \sqrt{\frac{\mu\varepsilon}{\mu_0\varepsilon_0}} = \sqrt{\frac{\varepsilon}{\varepsilon_0}}. \tag{2.16}$$

where we have applied our condition of non-magnetisation $\mu = \mu_0$. In our study, we employ only the $\mathbf{E_0^+}$ and $\mathbf{B_0^+}$ versions, and the refractive indices of our media are the same for all wavenumbers k (non-dispersive media).

PWs are infinite in spacetime, so they hardly represent a physical wave on their own, but due to their orthogonality they can be used as the Fourier components in the decomposition of a real wave, e.g. a light pulse, which is the approach we take in this project. Moreover, while the Poynting vector $\mathbf{S}$ of a PW is invariant in time and space, the $\mathbf{S}$ of a pulse does show variation, which is essential for fully employing eqn. (2.11).

2.6 Photonic Crystals

Photonic crystals (PCs) (fig. 2.1) are highly ordered materials that possess a periodically modulated dielectric constant, with the properties of confining and controlling the propagation of light generating a photonic band gap [25, 26].

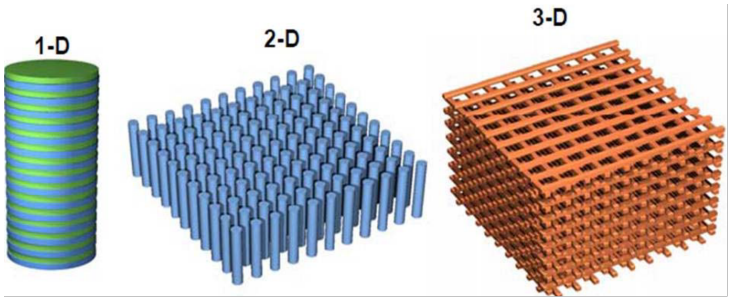

Figure 2.1: Schematic illustrations of *photonic crystal*s with simple periodic patterns. Taken from [27].

A common technique used when the periodicity of the crystal is much smaller than the wavelength of light is photonic crystal homogenisation, in which the macroscopic optical properties of PCs are treated as effective homogeneous media [28]. In this project, we aim instead to dehomogenise dielectric media and represent them as *photonic crystal*s, specifically as *periods* of thin medium and vacuum layers from which an effective refractive index n_{eff}, matching our desired dehomogenised medium can be calculated (sec. 3.2.4). This allows us to compute the MST in free space as all formulations are in agreement there. To avoid confusion, the italicised *medium* will be used from now on to refer exclusively to the medium *layers* of *photonic crystal*s *periods*, and the term *crystal* will be used to refer to the effective dielectric medium that we are dehomogenising into a *photonic crystal* (a chain of *periods*).

2.7 The Transfer Matrix Method

The transfer matrix method (TMM) is a mathematical formalism used in various fields to analyse the propagation of waves through layered structures or systems with spatially varying properties. It enables the efficient calculation of plane wave transmission and reflection coefficients for arbitrary angle of incidence θ and polarisation state and provides insights into the behaviour of waves as they propagate through the structure [29, 30]. In this study, we use s-polarisation (perpendicular to the plane of refraction), however, the study is polarisation independent as we limit ourselves to normal incidence $\theta = 0$ for simplicity.

The PWs are represented as ab-vectors which are composed of forward (a) and backward (b) propagating modes. These modes correspond to the electric part of an EM wave and are polarised along a given direction. They encapsulate the amplitude and the phase of the PWs at a particular position and moment in time. In a given medium with n, the magnetic part

$$\mathbf{B} = \frac{1}{\omega}\mathbf{k} \times \mathbf{E} \underset{\theta \overset{!}{=} 0}{=} \frac{n}{c}\hat{\mathbf{k}} \times \mathbf{E} \tag{2.17}$$

which is obtained from eqns. (2.3, 2.13, 2.14, and 2.15).

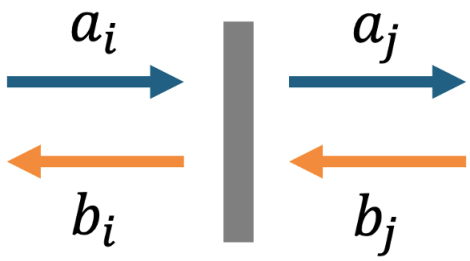

Figure 2.2: A diagram illustrating a scattering event on an optical *element* (grey rectangle) of electric field modes (a and b vectors). The subscripts i and j refer to positions relative to the *element*.

The optical system under consideration is composed of multiple *layers* with different properties (here just n) and the *interfaces* between them. The layer properties are expressed in matrix form, where there is a distinction between Scattering (S) and Transfer (M) matrices.

S matrices relate the input state and the output state of a physical system undergoing a scattering process [31]. They can be understood as being "event ordered" as the output states are the result of a physical process dictated by the properties of the matrix. With reference to fig. 2.2, the S matrix of this *element* and the transformation relation are

$$\underline{\underline{\mathbf{S}}}_{\mathbf{ij}} = \begin{pmatrix} r_{ij} & t_{ji} \\ t_{ij} & r_{ji} \end{pmatrix} \rightarrow \begin{pmatrix} b_i \\ a_j \end{pmatrix} = \underline{\underline{\mathbf{S}}}_{\mathbf{ij}} \begin{pmatrix} a_i \\ b_j \end{pmatrix} \tag{2.18}$$

where r_{ij} and t_{ij} are respectively the reflection and transmission coefficients experienced by a PW propagating from i to j. It is clear that a_i and b_j are the scattering inputs while a_j and b_i are the outputs.

On the other hand, M matrices are not event-ordered. They relate the wave's amplitude and phase on one side of the *element* to those on the other side [31]. Information about the outcome of the scattering process is required to use them. With reference to fig. 2.2, the M matrix of this *element* and the transformation relation are

$$\underline{\underline{\mathbf{M}}}_{\mathbf{ij}} = \begin{pmatrix} m_{ii} & m_{ij} \\ m_{ji} & m_{jj} \end{pmatrix} \rightarrow \begin{pmatrix} a_j \\ b_j \end{pmatrix} = \underline{\underline{\mathbf{M}}}_{\mathbf{ij}} \begin{pmatrix} a_i \\ b_i \end{pmatrix} \tag{2.19}$$

where m_{ij} are coefficients derived from r_{ij} and t_{ij} through linear analysis.

$$\begin{pmatrix} m_{ii} & m_{ij} \\ m_{ji} & m_{jj} \end{pmatrix} = \begin{pmatrix} t_{ij} - r_{ij}\frac{r_{ji}}{t_{ji}} & \frac{r_{ji}}{t_{ji}} \\ -\frac{r_{ij}}{t_{ji}} & \frac{1}{t_{ji}} \end{pmatrix} \Leftrightarrow \begin{pmatrix} r_{ij} & t_{ji} \\ t_{ij} & r_{ji} \end{pmatrix} = \begin{pmatrix} -\frac{m_{ji}}{m_{jj}} & \frac{1}{m_{jj}} \\ m_{ii} - m_{ij}\frac{m_{ji}}{m_{jj}} & \frac{m_{ij}}{m_{jj}} \end{pmatrix} \tag{2.20}$$

In S form, it is easier and more intuitive to input the reflection and transmission coefficients, but the matrix needs to be in M form if we wish to cascade the matrices of individual *elements* together or simply to know the overall field (superposition of a and b) at particular positions of the system if we know them at somewhere else already.

3. Numerical Implementation

3.1 Physical Dimensions and General Properties

As our main objective is to visualise physical behaviour, the real physical dimensions of objects are not of tremendous relevance in our study. Therefore, a number of physical constants (ε_0, μ_0, c) have been set to unity and we employ arbitrary units for our quantities. The refraction plane is the x-z plane so, because we work at normal incidence $\theta = 0$, s-polarised $\mathbf{E_0}$ points along $\hat{\mathbf{y}}$, $\mathbf{B_0}$ points along $\hat{\mathbf{x}}$ and, the direction of propagation is $\hat{\mathbf{z}}$ (pointing to the right).

3.2 Creating the Optical System

3.2.1 Fundamentals

The optical system that a given PW "sees" depends on its wavevector $\mathbf{k}$ as the angle of incidence θ affects the reflection and transmission coefficients at an *interface* and the magnitude of its wavevector components along the direction of propagation determines the phase shift a wave experiences when propagating through a medium. We work with an array of input wavenumbers $k = \frac{2\pi}{\lambda}$ (entering the system from vacuum) in a range such that the wavelengths λ in free space are always bigger than the *period* width h (even when reduced in a *medium*). Thus, for a series of *layers* with fixed n values, even though all PWs will experience the same reflection and transmission coefficients at the *interfaces*, they will undergo different phase shifts when propagating, so the chain of matrices representing the system needs to be reproduced each k.

At an interface where we know n_i and n_j of the *layers* i and j, given that the layers are oriented perpendicular to $\hat{\mathbf{z}}$, for an incident wavevector $\mathbf{k_i}$, the resulting wavevector $\mathbf{k_j}$ in *layer* j immediately after the *interface* is calculated as

$$\mathbf{k_j} = (k_{ix}, k_{iy}, \sqrt{k_{iz}^2 + |\mathbf{k_i}|^2 \left(\left(\frac{n_j}{n_i} \right)^2 - 1 \right)} \tag{3.1}$$

Thus, with this information, the S *interface* for interfaces can be constructed by exploiting the relations (independent of polarisation) [24]

$$r_{ij} = \frac{k_{iz} - k_{jz}}{k_{iz} + k_{jz}} \tag{3.2}$$

$$t_{ij} = \frac{2k_{iz}}{k_{iz} + k_{jz}} = 1 + r_{ij} \tag{3.3}$$

When propagating through a *layer*, we assume homogeneity such that there should be no reflection and all the wave is transmitted while picking up a phase shift. For a *layer* i with refractive index n_i and *layer* width h_i, the S matrix is

$$\overleftrightarrow{\mathbf{S}}_{\mathbf{ij}} = \begin{pmatrix} 0 & t_{ji} \\ t_{ij} & 0 \end{pmatrix} = \begin{pmatrix} 0 & e^{ik_{iz}h_i} \\ e^{ik_{iz}h_i} & 0 \end{pmatrix} \tag{3.4}$$

Following the relations in eqn. (2.20), we can switch between M and S forms computing composite matrices of a series of *elements* if required.

3.2.2 Composite Structure

A *crystal period* has 5 component *elements* (fig. 3.1): vacuum portion, *interface*, *medium* portion, *interface*, and vacuum portion. A *period* has a specified width h, and r, the fraction of the *period* that is vacuum (from hereon referred to as the width ratio), determines the width of the vacuum (rh) and *medium* ($(1-r)h$) portions. There are two vacuum portions, one at either side of the *period*, and both have equal width $\frac{rh}{2}$.

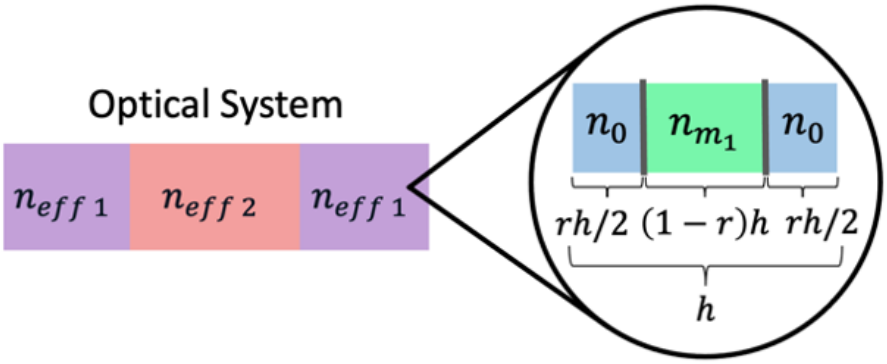

Figure 3.1: Simple diagram illustrating the microscopic composition of the simulated *photonic crystal*s in an example optical system. h is the *period* width, r is the width portion, n_0 is the vacuum refractive index, n_m is the medium refractive index, and n_{eff} is a *crystal's* effective refractive index. The blue blocks represent vacuum layers, while the green blocks represent *medium layers*, and the dark grey lines represent *interfaces* between them.

Our program takes the wavevectors in vacuum $\mathbf{k_i}$ and medium $\mathbf{k_j}$ (calculated from n_i and n_j) and the widths of the two portions $h_i = rh$ and $h_j = (1-r)h$, and produces the 5 component *elements* in S form, and the total S and M matrices of the full *period*. Since the *crystals* are made up of chains of identical *periods* (lists of the same 5 matrices), each PC type is specified uniquely by 4 variables: r, h, n_m and N_{per}, the number of *periods* in the *crystal*. Thus, with lists of these variables and the wavenumber values, we concatenate long chains of matrices representing whichever composite PC system we want for any PW with a given $\mathbf{k}$.

3.2.3 The Distributed Bragg Reflector

A distributed Bragg reflector (DBR) consists of periodic quarter-wavelength stacks of high and low refractive index materials [32] with the purpose of producing destructive interference between transmitted and reflected waves in consecutive *periods* such that the intensity is attenuated with propagation and most of the wave is reflected back - effectively a mirror.

We define a characteristic wavenumber k_{DBR}, that defines the physical structure of DBR, and a *medium* refractive index n_{DBR} such that the DBR will effectively reflect all PWs with

different wavenumbers. We employ a visual test fig. 3.2 which consists in plotting the modulus of the minimum of the two eigenvalues of a DBR *period* for the different wavenumbers varying k_{DBR} and n_{DBR} until none of the eigenvalues is close to 1, which would result in transmission. When the minimum eigenvalues correspond to the forward-propagating eigenvectors and their moduli are less than 1 this results in exponential decay over *periods* in the forward direction (evanescence) and exponential growth over in the backward direction (tending to full reflection).

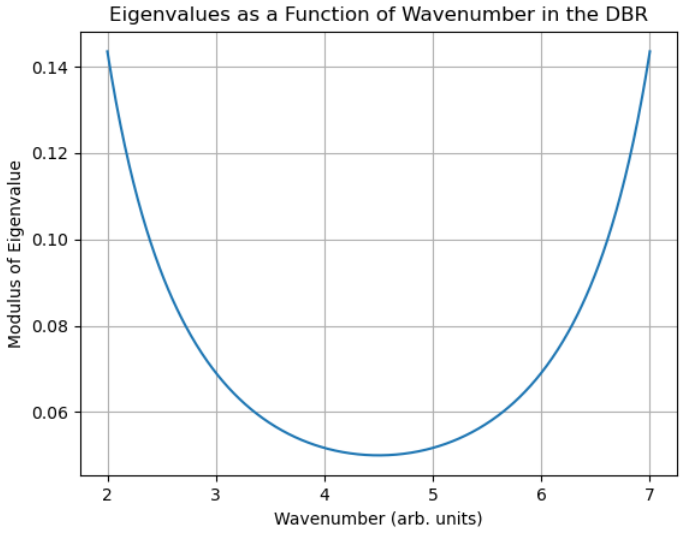

Figure 3.2: A plot of the modulus of the minimum eigenvalue of a single DBR *period* ($n_{DBR} = 20$ and $k_{DBR} = 4.50$) against incident wavenumber (in vacuum).

The chosen range for the wavenumbers k is from 2.00 to 7.00 in steps of 0.01. This range remains larger than the *period* widths chosen for the simulation while passing the test for a DBR with $n_{DBR} = 20$ and $k_{DBR} = 4.50$. The DBR matrices can be produced much in the same way as any other PC as the same input variables are required ($r = \frac{n_{DBR}}{1+n_{DBR}}$, $h = \frac{\pi}{2k_{DBR}}\left(1 + \frac{1}{n_{DBR}}\right)$, $n_m = n_{DBR}$, and $N_{per} = 10$).

3.2.4 Effective Media

We obtain a value for the effective index of refraction n_{eff} of a *period* with n_m by considering its forward-propagating eigenvalue ξ (from its M form) and treating it as a phase shift induced on a PW with wavevector $\mathbf{k_i}$

$$\xi = e^{ik_{iz}hn_{eff}} \tag{3.5}$$

Scaling it with the hypothetical phase shift $e^{ik_{iz}hn_m}$ induced by the *medium* part if it had the same width as *period* h, taking the log and dividing by $ik_{iz}h$,

$$\Delta n = \frac{1}{ik_{iz}h}\log\left(\frac{e^{ik_{iz}hn_{eff}}}{e^{ik_{iz}hn_m}}\right) = \frac{1}{ik_{iz}h}\log(e^{ik_{iz}h(n_{eff}-n_m)}) = n_{eff} - n_m \tag{3.6}$$

Adding this to n_m gives n_{eff}. Employing a root finding algorithm we calculate the n_m a *crystal period* requires for given n_{eff}, h, and r.

Other than the DBR, we work with 3 types of *crystals*. All 3 have $r = 0.01$, so *periods* are mainly *medium*, $h = 0.1$, which is smaller than all wavelengths, and $n_{eff} = 1.0, 1.5, 2.5$, which correspond to vacuum, SiO_2 and a TiO_2 (not at the same wavelengths) [33]. The corresponding $n_m = 1.0, 1.504, 2.511$.

3.3 Propagating the Fields

The method for obtaining the field amplitudes and phases consists of computing the eigenvectors at the right-hand end (exit) of the optical system and back-propagating them through the system.

```
1  def amps_from_emb_pol(a0_pol,emb,DBR_exist):
2      last_per = totalSM(emb[-5:])[1]
3      aibi_pol = np.empty((len(emb)+1,2),dtype=np.complex64)
4      if DBR_exist:
5          anbn_pol = evanescent_evec(last_per)
6      else:
7          anbn_pol = semi_inf_prop(last_per)
8      aibi_pol[-1] = anbn_pol
9      m = np.eye(2)
10     for i in range(len(emb)-1,-1,-1):
11         m = np.linalg.inv(StoM(emb[i]))@m
12         aibi_pol[i] = m@(anbn_pol)
13     return np.transpose(aibi_pol/aibi_pol[0][0])*np.abs(a0_pol)
```

Code 3.1: The back-propagation function.

The working principle behind code 3.1 - the core of the simulation - is as follows. `emb` contains all the matrices of the *elements* of the optical system which already encode a given wavevector **k**. An M matrix is formed out of the last 5 *elements* (forming a single *period*). These could pertain to a DBR or a vacuum (or really any *crystal*) *period*. An array `aibi_pol` is created to store the a and b values which is longer than `emb` by 1 because we also want to store the output vector. `DBR_exist` is a truth statement informing whether there is DBR at the end of the system. In case there is one, `evanescent_evec` selects the evanescent eigenvector by looking at the eigenvalues. In the case there is none, we assume that the last *crystal* (here vacuum) prolongs itself to infinity such that there is no *boundary* with a different *crystal* that would result in a back-reflection. This would mean that the output vector has to be the forward-propagating eigenvector of the last *period* in the system, which is selected by `semi_inf_prop` by looking at the a part of the eigenvectors. The output vector is placed at the end of `aibi_pol` and is back-propagated through the system by inverting each and every M matrix, cascading at each step, and operating on the output vector producing the amplitudes and phases at every *element*. Finally, all the vectors are normalised with respect to the a part of the vector at the left-hand end of the system (in theory, our input PW), so that the initial phase and amplitude are 0 and 1, though the latter can be re-scaled with `a0_pol` (this is there in case the simulation is elevated to a non-s-polarisation case where these amplitudes and phases only correspond to the s component part of a singly or multi-polarised wave).

For every wavevector $\mathbf{k}$, a structure with the system properties n_m, h, r, and N_{per} is produced and the waves at each position of the structure are generated and stored. Furthermore, a normalised Gaussian envelope is applied to weight the PW components as a function of their wavenumber k with central value $k_c = 4.50$ and width parameter $k_\sigma = 1.0$. This is essentially finding the Fourier transform of a pulse. Moreover, each array of wave values is tensor-multiplied by a time-varying complex exponential e^{-ickt}. This encodes the time dependence that we had so far neglected employing eqn. (2.15). Thus, we possess the amplitudes and phases for the waves at different positions in the system, at different moments in time, for different wavevectors.

3.4 The Maxwell Stress Tensor and Momentum Flux

The MST is computed employing the values of $\mathbf{E}$ and $\mathbf{B}$ at the edges of the *periods*, which are always in vacuum, so the MST from eqn. (2.12) can be used. The total $\mathbf{E}$ and $\mathbf{B}$ (through eqn. (2.17)) at a position and time are given by the superposition of the forward and backward-propagating waves at those coordinates. Hence, computing $\overleftrightarrow{\mathbf{T}}$ involves considering the interference between PWs of different wavenumber and propagation direction. However, exploiting the properties of PWs at normal incidence, analytically solving for the elements of the MST and projecting it onto the z-direction results in a simple and computationally efficient expression for the z-component of the MST $\mathbf{T^z}$. At a fixed time t, at an *element* l,

$$\mathbf{T^z}_{tl} = -\frac{n_l^2}{\mu_0} \sum_k \sum_{k'} kk' \Re \left(a^*_{tlk} a_{tlk'} + b^*_{tlk} b_{tlk'} \right) \tag{3.7}$$

where n_l is the refractive index at *element* l, and k, k' indicate a plane wave's wavenumber. a/b_{tlk} gives an a or b component at a specified time t, element l and wavenumber k.

With reference to eqn. (2.11) and the Divergence Theorem, we calculate the rate of momentum flow $\frac{d\mathbf{p}}{dt}$ (the force) into the *medium layers* by performing a surface integrals over the MSTs centred at the middle of the *medium layers*. Since we know the values of $\overleftrightarrow{\mathbf{T}}$ at the *period* edges we place our integration surface there. The normal vectors to the plane parallel layers are $-\hat{\mathbf{z}}$ for the layer to the left and $\hat{\mathbf{z}}$ for the layer to the right. Because this is a 1D problem, there are no surface areas, so all we can do is project the $\overleftrightarrow{\mathbf{T}}$ and obtain momentum fluxes $\mathbf{\Pi} = \frac{1}{A}\frac{d\mathbf{p}}{dt}$ rather than rates of momentum. For a *medium layer* i at a time t,

$$\mathbf{\Pi}_{ti} = \oiint_W \overleftrightarrow{\mathbf{T}}_{ti} \cdot d\mathbf{W} \Rightarrow \overleftrightarrow{\mathbf{T}}_{ti_vL} \cdot (-\hat{\mathbf{z}}) + \overleftrightarrow{\mathbf{T}}_{ti_vR} \cdot \hat{\mathbf{z}} = \mathbf{T^z}_{ti_vR} - \mathbf{T^z}_{ti_vL} \tag{3.8}$$

where W is the integration surface, and $d\mathbf{W}$ is the surface element. L and R indicate whether we mean the vacuum *layer* to the left or the right of the *medium layer*. The subscript v on the is indicates that these are the values of the $\overleftrightarrow{\mathbf{T}}$ at the edges of a *period* i which are in the vacuum portion. We project $\mathbf{\Pi}_{ti}$ onto $\hat{\mathbf{z}}$ to obtain the momentum flux into the *medium* in the z-direction $\Pi^z{}_{ti}$.

3.5 Lorentz Bulk Forces

As we work in 1D with normal incidence, $\mathbf{E}$ always points perpendicular to the propagation direction. Thus, the first terms on the RHS of eqns. (2.8) & (2.9) vanish leaving the same expression

$$\mathbf{f_v} = \frac{\partial \mathbf{P}}{\partial t} \times \mathbf{B} \tag{3.9}$$

where, via eqn. (2.16), we can employ

$$\mathbf{P} = \varepsilon_0(n^2 - 1)\mathbf{E} \tag{3.10}$$

As $\mathbf{E}$ is given by the sum of the component PWs, $\frac{\partial \mathbf{P}}{\partial t}$ will be $\varepsilon_0(n^2-1)$ times the sum of each a and b component multiplied by $i\omega$ where ω is different for each ab pair due to eqn. (2.15). Taking the cross product with $\mathbf{B}$ requires a consideration of the interference between as and bs of different wavenumber and signs. Exploiting the properties of PWs at normal incidence, employing time-averaging methods for complex fields, analytically solving for the cross product and integrating over the width of the *medium layer* of each *period* delivers a Lorentz force surface density $\mathbf{f_s}$ (for comparison with MST momentum flux) in each period. At layer j and time t,

$$\begin{aligned}\mathbf{f_s}_{tj} = \frac{n_j^2 - 1}{2\mu_0} \sum_k \sum_{k'} kk' \Re \Big[&\left(1 - e^{-ih_j(k-k')n_j}\right) a^*_{tjk} a_{tjk'} - \left(1 - e^{-ih_j(k+k')n_j}\right) a^*_{tjk} b_{tjk'} \\ &- \left(1 - e^{ih_j(k+k')n_j}\right) b^*_{tjk} a_{tjk'} + \left(1 - e^{ih_j(k-k')n_j}\right) b^*_{tjk} b_{tjk'} \Big]\end{aligned} \tag{3.11}$$

where n_j and h_j give the refractive index and *layer* width in *layer* j. The physical position specified by j is at the LHS within the *medium layer* (right next to the *interface*).

3.6 Impulse Time Graphs

We calculate $\Delta\eta^z$ the accumulated impulse surface density along $\hat{\mathbf{z}}$ through both the MST and the Lorentz force methods. Impulse is the integral of momentum flow rate (or force) over time, so for MST

$$\Delta\eta^z(t) = \int_{t_0}^{t} \Pi^z(t')dt' \Rightarrow \sum_{t'=t_0}^{t} \Pi^z(t')\Delta t \tag{3.12}$$

and for Lorentz

$$\Delta\eta^z(t) = \int_{t_0}^{t} \mathrm{f}_s^z(t')dt' \Rightarrow \sum_{t'=t_0}^{t} \mathrm{f}_s^z(t')\Delta t \tag{3.13}$$

The time-step Δt (here $= 0.05$ due to computational limitations) chosen must be small enough that Π_z and f_s^z are relatively smooth (smaller than $\frac{2\pi}{\omega}$). Computationally, $\Delta\eta^z{}_i$ as a function

of time at a position i is calculated as a cumulative sum along the time axis. Moreover, for calculating the total impulse surface density imparted on a macroscopic portion of the system (*crystals*, DBR, etc.) we sum over the range of *periods* corresponding to a chosen portion, as if all the impulse was imparted to the centre of mass of that portion of the system.

In order to have a notion of how much $\Delta\eta^z$ has been imparted we normalise with respect to the original momentum surface density of the pulse η_0. This is measured by running a simulation where the pulse propagates through vacuum, is reflected off the DBR, and the $\Delta\eta^z$ imparted on the DBR is measured. This is effectively twice η_0 for total reflection.

Finally, in order to test eqn. (2.11), we compute the Poynting vector contribution also employing time-averaging methods and simplifying through the interference terms due to the cross product and time derivatives as in sec. 3.5. Furthermore, we integrate $\mathbf{S}$ over a volume reaching the edges of a *period* (same integration limits as for the MST), but again because of the 1D constrain this turns into a projection onto $\hat{\mathbf{z}}$ and a line integral over the *period* width. Over a *layer* j,

$$\int \frac{\partial \mathbf{S}_j}{\partial t} \cdot \hat{\mathbf{z}} dz = \frac{1}{\mu_0} \sum_k \sum_{k'} \Re\Bigg[\left(1 - e^{ih_j(k-k')n_j}\right) a^*_{tjk} a_{tjk'} - \frac{k-k'}{k+k'} \left(1 - e^{ih_j(k+k')n_j}\right) a^*_{tjk} b_{tjk'} + \frac{k-k'}{k+k'} \left(1 - e^{-ih_j(k+k')n_j}\right) b^*_{tjk} a_{tjk'} - \left(1 - e^{-ih_j(k-k')n_j}\right) b^*_{tjk} b_{tjk'} \Bigg] \quad (3.14)$$

$\Delta\eta^z(t)$ is then calculated in the usual way as above. Because of the $\frac{1}{c^2}$ factor, we need a measure of the propagation speed of our pulse in vacuum. This is determined with the same simulation in vacuum from above using a peak-finding algorithm and a Gaussian fit for tracking the centre of the pulse over position and time. Unsurprisingly, this gives a value of $c \approx 1$.

4. Results and Discussion

In all the graphs that appear next, the colour coding is the following: light blue background = vacuum, red bkgd. = *crystal* (called 1) with $n_{eff} = 1.5$, green bkgd. = *crystal* (called 2) with $n_{eff} = 2.5$, vertical black dashed lines = *boundaries* between *crystals*, vertical black thick line = DBR *boundary*, and grey bkgd. = DBR structure.

4.1 Intensities

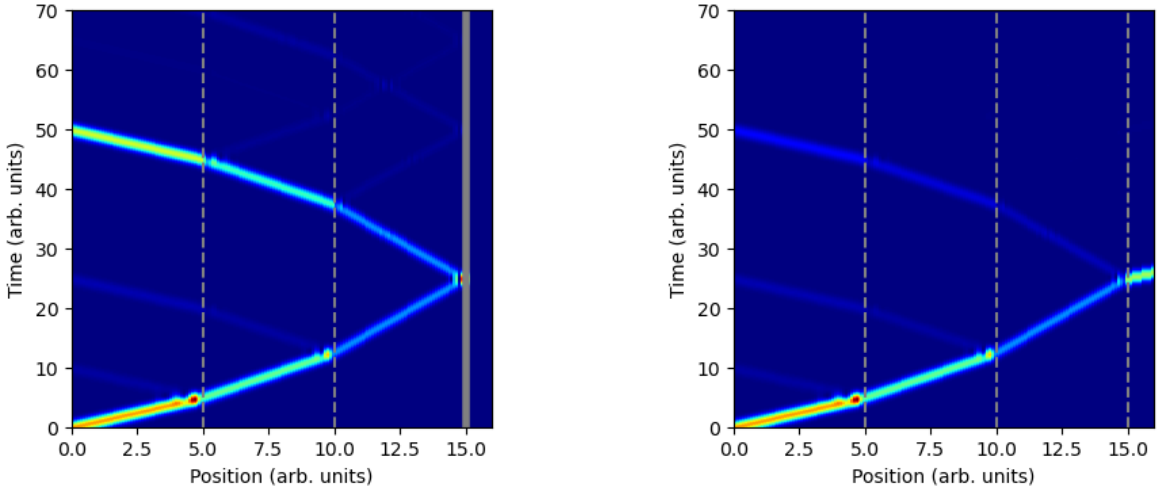

(a) DBR structure case.

(b) Vacuum case.

Figure 4.1: Pulse intensities as a function of time and position for the system with (a) a DBR structure at the end and (b) vacuum at the end. The dashed lines represent *boundaries* between crystals and the continuous line represents a *boundary* with the DBR.

In fig. 4.1, the two optical system cases are illustrated with reflection time near $t = 26.00$ arb. units. In fig. 4.1a is shown the case with the DBR structure at the end and it is visible that the pulse is reflected. A finite portion of the pulse intensity enters the DBR but vanishes ~ 2 *periods* in displaying its function as a fully reflective mirror. In fig. 4.1b is shown the case with vacuum at the end. In this case, the pulse is partially transmitted and leaves the simulation but a small portion is reflected back at the *crystal* 2 - vacuum *boundary*.

Before encountering the DBR, both cases show identical intensities. In fig. 4.2, the back-reflections in the *crystals* results in an attenuated total field intensity. Since in all formulations of the momentum density it is parallel with the field propagation, these results would suggest Abraham-like behaviour in that the EM momentum should see a reduction in a dielectric medium (in the common sense, not the *period* layer). However, upon comparing relative total intensities (integrating the pulses) and relative peak intensities no direct relation can be found with the effective crystal refractive indices n_{eff}.

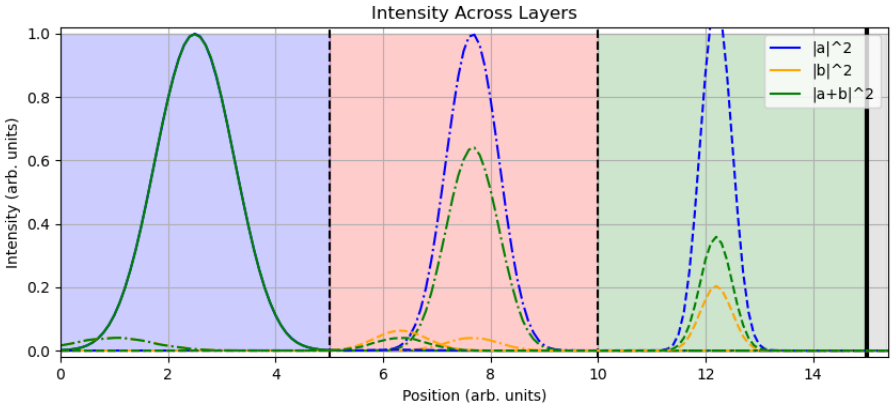

Figure 4.2: Intensities at $t = 2.50$ arb. units (full line), $t = 9.00$ (dot-dash line), and $t = 18.00$ (dashed line).

4.2 The Maxwell Stress Tensor (momentum fluxes)

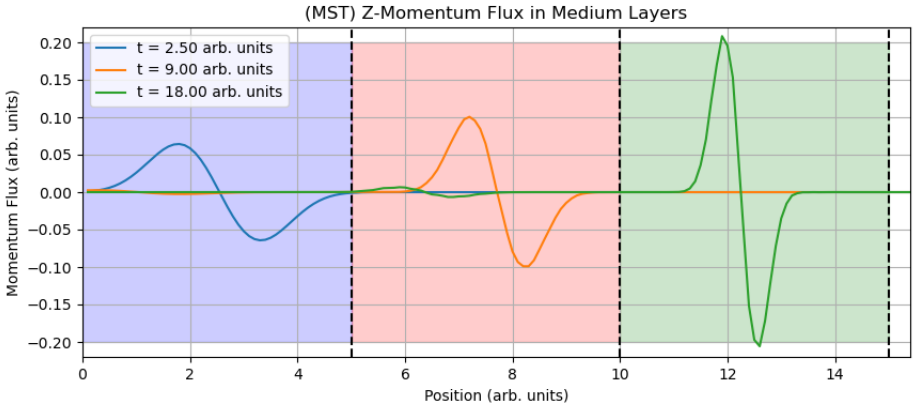

Figure 4.3: $\hat{\mathbf{z}}$ momentum fluxes at 3 different times before encountering the final *boundary*.

Before encountering the DBR, both cases show identical $\hat{\mathbf{z}}$ momentum fluxes. In fig. 4.3, it is notable that upon entering a *crystal* with a higher n_{eff} the waves of $\hat{\mathbf{z}}$ momentum flux become narrower (as expected for a slower group velocity in a higher n_{eff}) and their peaks obtain greater amplitudes. These results would suggest Minkowski-like behaviour in that the EM momentum should see an increase in a dielectric medium (in the common sense, not the *period* layer). Once again, however, there is no direct relation between effective *crystal* refractive indices n_{eff} and the peak sizes.

In fig. 4.4, we compare the $\hat{\mathbf{z}}$ impulse surface density at the long-time limit between the two cases. In both, the impulse accumulates at the *boundaries* between crystals, while in the bulk it tends to 0, although there are transient build ups due to interference between transmitted and reflected waves. The leftover impulses in the bulks are likely due to numerical errors originating at the finite value of the time-step Δt. It is worth noting that a massive amount of impulse is accumulated at the DBR. The DBR case has overall more impulse accumulated as a result of the additional more intense reflected pulses going back into the structure after reflection.

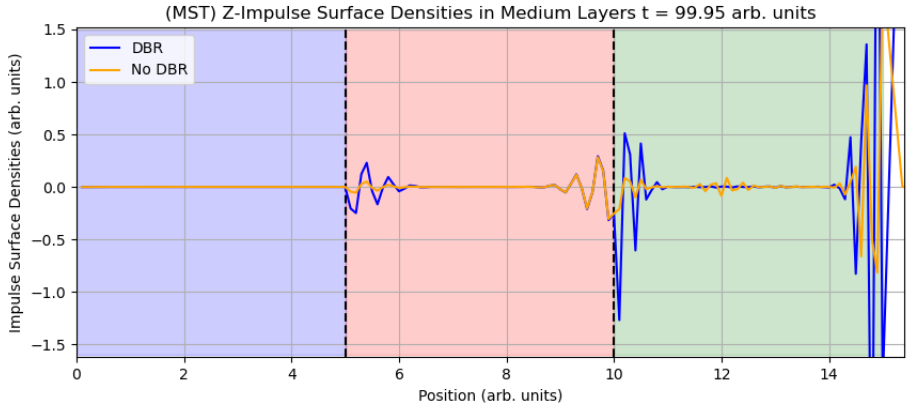

Figure 4.4: The $\hat{\mathbf{z}}$ impulse surface densities, calculated via the Maxwell stress tensor method, at the long-time limit for both the mirror and vacuum cases. (No final *crystal* shown as this data pertains to both cases).

It makes sense, given the symmetry of the pulse, that the overall impulse in the bulk should be 0 since, as the pulse propagates through a period, the divergence of the $\overleftrightarrow{\mathbf{T}}$ "seen" by that period should perfectly cancel out. This symmetry of the pulse is broken as there is a change of *crystal*, which is why integrating over time does not simplify to 0.

4.3 The Lorentz Force

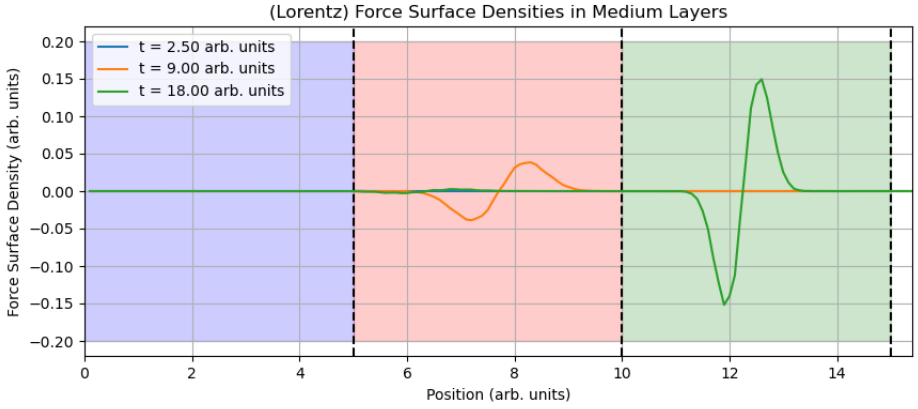

Figure 4.5: $\hat{\mathbf{z}}$ Lorentz force surface densities at 3 different times before encountering the final *boundary*.

Before encountering the DBR, both cases show identical $\hat{\mathbf{z}}$ Lorentz force surface densities. In fig. 4.5, we see that in vacuum there is no Lorentz force, which makes sense as there is no dielectric medium to polarise. However, in the *crystals*, we see identical behaviour to that in sec. 4.2 i.e. Minkowski-like but with no direct relation between effective crystal refractive indices n_{eff} and the peak sizes.

Looking at fig. 4.6, it is notable that, in the long term limit, the $\hat{\mathbf{z}}$ impulse surface density left behind is similar to the one in sec. 4.2 for both the mirror and no mirror cases. In this case,

the lack of build up in the bulk arises because the pulse is symmetric over time everywhere except at the crystal *boundaries* where there would be difference.

Nonetheless, the transient behaviour of the Lorentz and MST methods differ, namely in magnitude, before the long-time limit. This is illustrated in the next section.

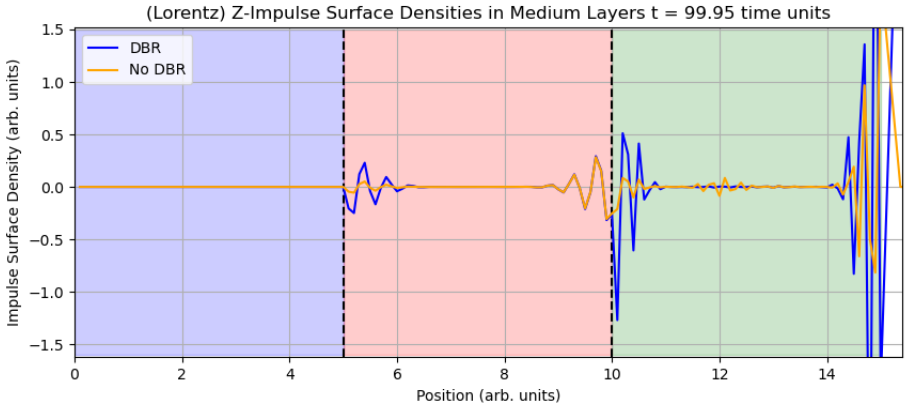

Figure 4.6: The $\hat{\mathbf{z}}$ impulse surface densities, calculated via the Lorentz force method, at the long-time limit for both the mirror and vacuum cases. (No final crystal as this pertains to both cases).

4.4 Impulse Over Time

In fig. 4.7, we have plotted essentially the two sides of eqn. (2.11), but with the Poynting vector term moved to the LHS. We remark that, both methods deliver the same total impulse surface densities in the long-time limit in the 2 *crystals* but not in the DBR. At the moment of submission, this phenomenon remains unexplained and investigating would be the first order of business if time allowed. Nevertheless, in all parts of the system the transient behaviour is markedly different for the two methods. The Lorentz forces contribute impulses to the whole system at all *boundary* interactions while the MST contribution depends more on bulk interactions (the pulse leaves or enters system). This makes sense because of the way the momentum flux is calculated in the MST method. The projection of the $\overleftrightarrow{\mathbf{T}}$ at the *period* and subsequent differentiation should result in cancellation everywhere but at the edges of integration for any given spatial integral. Moreover, the disagreement between both methods in terms of magnitude can be explained through the non-uniqueness of the MST sec. 2.4, which has no effect on the long-term limit. Once again, there appears to be no connection between the relative magnitudes of these impulses and the effective refractive indices. Removing the $\mathbf{S}$ term shifts the transient MST curve but has no impact on the long-time limit. This is to be expected as we are integrating a derivative with respect to time over time, so only the initial and final values of $\mathbf{S}$ should matter, and since energy is conserved, the global value of $\mathbf{S}$ has to remain constant and once the pulse leaves the system so does the energy. The speed of light c, even in a dielectric medium, is much larger than the speed of the acoustic waves in the material, meaning that the mechanical response could only "see" the overall impulse transfer rather than the transient behaviour. Experimentally, it is only this total impulse which we could measure.

The DBR accumulates more than twice the initial momentum for the MST method. This is because there are multiple reflections at the *boundaries* resulting in more smaller pulses arriving at the DBR and being fully reflected there. Depending on the transmission coefficients at other *boundaries*, it could have been the case that the DBR accumulated less than twice the initial momentum as only a much smaller fraction would have arrived at the DBR.

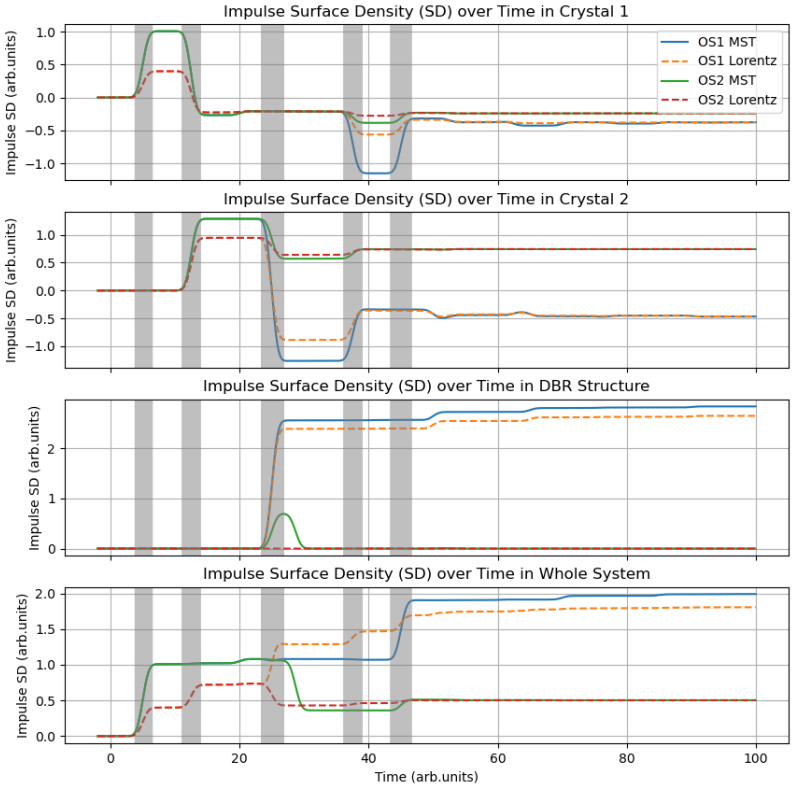

Figure 4.7: The total $\hat{\mathbf{z}}$ impulse surface densities in different sections of the optical systems as a function of time. The $\mathbf{S}$ term has been subtracted from the MST term. The grey bands mark times when major *boundary* interactions take place. In order from left to right: pulse enters *crystal* 1, pulse enters *crystal* 2, pulse hits mirror/exits system, main reflected pulse re-enters *crystal* 1, and main reflected pulse exits the system going left.

Nevertheless, the total impulse given to the whole system is exactly twice the initial momentum for the DBR case (only for the MST). This is to be expected since, by the time the pulse has fully left the system, it has the same amount of momentum as it did at the beginning of the simulation but in the opposite direction, so the system must now have twice that amount in the original direction to conserve momentum.

5. Conclusion

In this project, we have developed computational tools to visualise the field momentum of light waves travelling in dielectric media. We simulated optical media as 1D *photonic crystal*s composed of *periods* of thin medium and vacuum *layers*, and employed the TMM to find the electric and magnetic fields of a pulse composed of s-polarised PWs at the different *elements* of the system. We simulated two optical systems: one corresponds to 2 *crystals* sandwiched between a vacuum section and a DBR structure acting as a mirror and the other corresponds to the same *crystals* between two vacuum sections. Visualising the intensities in the different *crystals* revealed a reduction with increasing effective refractive index as suggested by Abraham, although an exact dependence could not be determined.

In both optical systems, we computed the MST at the vacuum *layers* and the Lorentz force acting on the bulk of *medium* and vacuum *layers*. This allowed the calculation of the momentum fluxes and force surface densities acting on the medium parts of the system, revealing an enhancement with increasing effective refractive index as suggested by Minkowski, though not with the predicted linear dependence.

Additionally, the two momentum methods enabled calculating the accumulated impulse surface density in the systems yielding identical total impulses for the *crystals* but not the DBR and with transient disagreements. The latter behaviour can be explained by the non-uniqueness of the MST.

Our simulations correctly conserve momentum for the MST calculation and allow the creation and testing of a variety of media through the input of a few simple variables. However, high temporal and spatial resolution are very efficiency and memory heavy, which demands optimisation of the code.

5.1 Opportunities for Future Work

- It is worthwhile investigating the disagreement between the Lorentz and MST methods in the long time limit with care to examine why they differ at the DBR specifically. This may be because the DBR has really small r compared to the other *photonic crystal*s, but why this would affect the Lorentz force in this way is unknown.

- The simulation was simplified by only considering a 1D optical system with an s-polarised pulse at normal incidence. An extension could be to simulate 3D photonic crystals and observe birefringence effects with illumination from multiple angles of incidence and different pulse shapes.

- The refractive indices were made independent of wavelength, which is unphysical for most materials. Programming this dependence would bring the simulation closer to real world physics.

- The simulated system was made infinitely stiff in that it could accumulate impulse without any mechanical reaction. An addition to the simulation would be to give the layers an effective mass and spring constants between them to observe how the mechanical and EM momenta couple to each other.

References

[1] H. Krüger and E. Grün, "Chapter 29 - dust in the solar system," in *Encyclopedia of the Solar System (Third Edition)* (T. Spohn, D. Breuer, and T. V. Johnson, eds.), pp. 657–682, Boston: Elsevier, third edition ed., 2014. [Cited on page 1]

[2] O. Darrigol, "Poincaré and the reaction principle in electrodynamics," *Philosophia Scientiæ*, vol. 27, no. 2, pp. 63–125, 2023. [Cited on page 1]

[3] B. A. Kemp, "Resolution of the abraham-minkowski debate: Implications for the electromagnetic wave theory of light in matter," *Journal or Applied Physics*, vol. 109, p. 111101, jun 2011. [Cited on page 1]

[4] C. Baxter and R. Loudon, "Contributions of john henry poynting to the understanding of radiation pressure," *Proc. R. Soc.*, vol. 468, no. 2143, p. 1825–1838, 2012. [Cited on page 1]

[5] M. Abraham, "Zur elektrodynamik bewegter körper," *Rend. Circ. Matem. Palermo*, vol. 28, p. 1–28, 1909. [Cited on page 1]

[6] H. Minkowski, "Die grundgleichungen für die elektromagnetischen vorgängein bewegten korpern," *Nachrichten von der Gesellschaft der Wissenschaften zu Göttingen, Mathematisch-Physikalische Klasse*, vol. 1, p. 53–111, 1908. [Cited on page 1]

[7] B. Anghinoni, G. Flizikowski, L. Malacarne, M. Partanen, S. Bialkowski, and N. Astrath, "On the formulations of the electromagnetic stress–energy tensor," *Annals of Physics*, vol. 443, p. 169004, 2022. [Cited on pages 1 and 4]

[8] R. N. C. Pfeifer, T. A. Nieminen, N. R. Heckenberg, and H. Rubinsztein-Dunlop, "Colloquium: Momentum of an electromagnetic wave in dielectric media," *Rev. Mod. Phys.*, vol. 79, pp. 1197–1216, Oct 2007. [Cited on page 1]

[9] P. W. Milonni and R. W. Boyd, "Momentum of light in a dielectric medium," *Adv. Opt. Photon.*, vol. 2, pp. 519–553, Dec 2010. [Cited on pages 1, 2, and 4]

[10] G. Feng and J. Huang, "A heuristic resolution of the abraham–minkowski controversy," *The European Physical Journal Plus*, vol. 136, May 2021. [Cited on page 1]

[11] J. Chen and Q. Kougong, "Energy and momentum of electromagnetic waves in media," *Journal of Optics*, April 2023. [Cited on page 1]

[12] C. Baxter and R. Loudon, "Radiation pressure and the photon momentum in dielectrics," *Journal of Modern Optics*, vol. 57, no. 10, pp. 830–842, 2010. [Cited on page 1]

[13] A. Ashkin and J. M. Dziedzic, "Radiation pressure on a free liquid surface," *Phys. Rev. Lett.*, vol. 30, pp. 139–142, Jan 1973. [Cited on page 1]

[14] H. Choi, M. Park, D. Elliott, , and K. Oh, "Optomechanical measurement of the abraham force in an adiabatic liquid-core optical-fiber waveguide," *Phys. Rev. A*, vol. 95, p. 053817, May 2017. [Cited on page 1]

[15] G. Verma, V. Kumar, and W. Li, "Revealing light momentum in dielectric media through standing-wave radiation pressure," *Phys. Rev. A*, vol. 108, p. 043514, Oct 2023. [Cited on page 1]

[16] D. J. Griffiths, "Resource letter em-1: Electromagnetic momentum," *Am. J. Phys.*, vol. 80, no. 1, p. 7–18, 2012. [Cited on page 1]

[17] A. B. C, "0.5.2 electromagnetic waves," in *Modern Problems in Classical Electrodynamics* (T. Spohn, D. Breuer, and T. V. Johnson, eds.), pp. 20–21, New York: OUP, 2004. [Cited on pages 2 and 4]

[18] D. Griffiths, "5.1 the lorentz force law," in *Introduction to Electrodynamics* (A. Reeves and K. Dellas, eds.), pp. 210–223, New Jersey: Prentice Hall, fourth edition ed., 2012. [Cited on page 3]

[19] M. Mansuripur, A. R. Zakharian, and J. V. Moloney, "Equivalence of total force (and torque) for two formulations of the Lorentz law," in *Optical Trapping and Optical Micromanipulation III* (K. Dholakia and G. C. Spalding, eds.), vol. 6326, p. 63260G, International Society for Optics and Photonics, SPIE, 2006. [Cited on page 3]

[20] S. M. Barnett and R. Loudon, "On the electromagnetic force on a dielectric medium," *Journal of Physics B: Atomic, Molecular and Optical Physics*, vol. 39, p. S671, jul 2006. [Cited on page 3]

[21] J. C. Shane, M. Mazilu, W. M. Lee, and K. Dholakia, "Effect of pulse temporal shape on optical trapping and impulse transfer using ultrashort pulsed lasers," *Opt. Express*, vol. 18, pp. 7554–7568, Mar 2010. [Cited on page 3]

[22] J. C. Maxwell, *A Treatise on Electricity and Magnetism*, vol. 1. Oxford: Clarendon Press, 1873. [Cited on page 3]

[23] D. Griffiths, "8.2 momentum," in *Introduction to Electrodynamics* (A. Reeves and K. Dellas, eds.), pp. 362–364, New Jersey: Prentice Hall, fourth edition ed., 2012. [Cited on page 3]

[24] D. Griffiths, "9.3 electromagnetic waves in matter," in *Introduction to Electrodynamics* (A. Reeves and K. Dellas, eds.), pp. 401–410, New Jersey: Prentice Hall, fourth edition ed., 2012. [Cited on pages 4 and 7]

[25] J. Shao, G. Liu, and L. Zhou, "12 - biomimetic nanocoatings for structural ccloration of textiles," in *Active Coatings for Smart Textiles* (J. Hu, ed.), Woodhead Publishing Series in Textiles, pp. 269–299, Woodhead Publishing, 2016. [Cited on page 5]

[26] E. Yablonovitch, "Photonic crystals," *Journal of Modern Optics*, vol. 41, pp. 173–194, Dec 1994. [Cited on page 5]

[27] S. Robinson and R. Nakkeeran, "Photonic crystal ring resonator based optical filters," in *Advances in Photonic Crystals* (V. M. Passaro, ed.), ch. 1, Rijeka: IntechOpen, 2013. [Cited on page 5]

[28] J. Méndez, B. Mateo, and M. M. et al., "Homogenization method for one-dimensional photonic crystals with magnetic and chiral inclusions," *Eur. Phys. J. B.*, vol. 93, Jul 2020. [Cited on page 5]

[29] C. Troparevsky, A. S. Sabau, A. R. Lupini, and Z. Zhang, "Transfer-matrix formalism for the calculation of optical response in multilayer systems: from coherent to incoherent interference," *Opt. Express*, vol. 18, pp. 24715–24721, Nov 2010. [Cited on page 5]

[30] T. G. Mackay and A. Lakhtakia, *The Transfer-Matrix Method in Electromagnetics and Optics*. MorganClaypool, 2020. [Cited on page 5]

[31] Z. Zhu and C. Zheng, "Differentiable scattering matrix for optimization of photonic structures," *Opt. Express*, vol. 28, pp. 37773–37787, Dec 2020. [Cited on page 6]

[32] R. Ratajczak, J. Gaca, W. Wójcik, A. Stonert, K. Pągowska, J. Borysiuk, and A. Turos, "Structural analysis of distributed bragg reflector mirrors," *Vacuum*, vol. 83, pp. S148–S151, 2009. Proceedings of the seventh International Conference on Ion Implantation and other Applications of Ions and Electrons (ION 2008),16-19 June 2008, Kazimierz Dolny, Poland. [Cited on page 8]

[33] M. Polyanskiy, "Refractiveindex.info database of optical constants," *Sci Data*, vol. 11, no. 94, 2024. [Cited on page 10]